Solid Freeform Fabrication 2023: Proceedings of the 34th Annual International Solid Freeform Fabrication Symposium – An Additive Manufacturing Conference
Reviewed Paper

MULTI-BEAD AND MULTI-LAYER PRINTING GEOMETRIC DEFECT IDENTIFICATION USING SINGLE BEAD TRAINED MODELS

N. A. Surovi and G. S. Soh

Engineering Product Development, Singapore University of Technology and Design, Singapore, 487372

Abstract

In Wire Arc Additive Manufacturing (WAAM), a geometric defect is a defect that creates voids in the final printed part due to incomplete fusion between two non-uniform overlapping bead segments. Such a defect poses the onset of a severe problem during multi-bead prints. In our earlier work, a methodology has been developed to construct machine learning (ML)-based models to identify geometrically defective bead segments using acoustic signals. In this paper, we investigate the performance of these single-bead segments trained defect detection model scalability for identifying voids during multi-bead prints. A comparative study of the performance of a variety of ML models is explored based on Inconel 718 material printing. The results show that the single bead segments-based defect identification model can effectively identify defective and non-defective segments in both single-layer multi-bead printing and multi-layer multi-bead printing.

Introduction

Wire Arc Additive Manufacturing (WAAM) is an arc-welding-based additive manufacturing technique where weld beads are deposited layer-by-layer to form 3D metallic components [1, 2]. WAAM employs an electric arc as the heat source and metal wires as a material feedstock to fabricate parts. During the fabrication process, an electric arc melts the metal wire within a shielded environment provided by gas such as argon or helium. Using a shielding gas reduces the potential for contamination, helps with the material transfer, and protects the molten pool and its surroundings from oxidation [4]. WAAM features a high deposition rate suitable for fabricating moderate to large-scale components. Furthermore, it is a low-cost, environmentally friendly approach with a high material utilization ratio. This makes such an approach advantageous over alternative additive manufacturing processes, especially in the aerospace, oil, gas, and offshore marine industries [14, 15]. WAAM has become a promising fabrication process for various engineering materials such as titanium, aluminium, nickel alloy, steel, and bronze [12].

WAAM technologies have faced different challenges. Defects, such as lack of fusion, porosity, cracks, distortion, oxidation, etc., limit the accuracy achievable in the deposition process. These defects reduce the strength of the final printed product, thus affecting its lifespan and performance. Hence, it is important to identify the defective printing process correctly. This paper focuses on detecting geometrically defective segments, or geometric defects, that create voids in the final printed part due to incomplete fusion between two non-uniform overlapping bead segments. Such a defect needs to be better studied in the literature, and it poses the onset of a severe problem during multi-bead prints [8, 9].

Numerous non-destructive techniques have been employed in the literature to sense defects, such as acoustic signals, X-ray radiation, image, thermal measurement, etc. [16]. Among these, acoustic-based sensing has the advantage of low cost and shows the most potential to identify both external and internal defects. The acoustic sound generated by the electric arc comes from the pulsation of the electric arc and the

vibration of the weld pool metal [13]. Several works explored the relationships between the geometry of beads and the properties of acoustic signals [3]. Polajnar et al. [7] showed that irregularities in the bead geometry are reflected in the intensity of acoustic signals. Pal et al. [6] showed that acoustic signals could identify metal transfer modes and weld defects. Lv et al. [5] showed that the height of the arcs constituting the shape of the bead has a linear relationship with the pressure of the acoustic signal. The relationships mentioned above between the properties of the bead geometry and the measured acoustic signals inspire us to extract and use acoustic features to capture the geometric defects of the WAAM with appropriate feature-based models.

In our earlier work, we have developed a methodology to construct machine learning (ML)- based models to identify geometrically defective bead segments using acoustic signals for the WAAM process. The proposed methodology uses a heuristic dataset labeling approach to identify good and bad bead segments based on a variety of bead geometrical and process-related metrics. The heuristic search is performed by finding threshold values for these metrics that minimize the overlapping area between the Kernel Density Estimation (KDE)s formed by the distribution of the good and defective bead segments [10, 11].

In this paper, we investigate the performance of these single-bead segments trained defect detection model performance in identifying geometric defects during multi-bead prints. A comparative study of the performance of a variety of ML models is conducted. Experiments are carried out on Inconel 718 material based on two raster printing. One is based on single-layer multi-bead printing, and the another is based on multi-layer multi-bead printing. The results show that the single bead segments-based defect identification model can effectively be extended to identify defective and non-defective segments for multi-bead prints.

Experimental Procedure

Overview

Figure 1 gives an overview of the experimental approach. First, we collect acoustic signals from two different printing which we call the testing samples, i) single-layer multi-bead printing and ii) multi-layer multi-bead printing. Then we divide the whole acoustic signal of each testing sample into several segments. After that, we extract twelve-time domain features from each acoustic signal segment whose names and formulas are listed in Table 2.

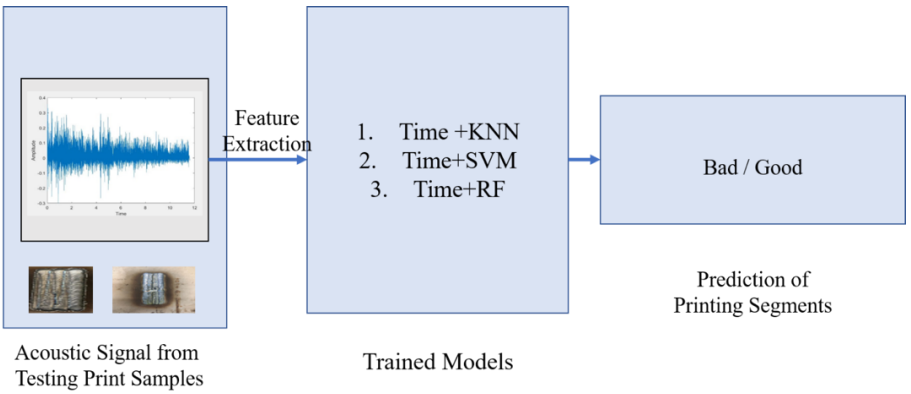

Figure 1: Overview of defect identification

Then we pass all signal features to three of our previously trained single bead segments ML models. These were trained based on K-Nearest Neighbor (KNN), Support Vector Machine (SVM), and Random Forest (RF). Finally, these trained models are evaluated based on their prediction of the quality of the printed multi-bead samples.

Experimental Setup

The experiments were conducted on our robotic WAAM system at the Singapore University of Technology and Design (SUTD), as shown in Figure 2. The system consists of a robot manipulator (ABB IRB1660ID), a welding power source (Fronius TPS 400i) equipped with a welding torch (Fronius WF 25i Robacta Drive), a cartesian coordinate robot made up of three linear rails (PMI KM4510) powered by three servos (SmartMotor SM34165DT), and a microphone (UMIK-1 miniDSP) installed at around 80 cm above the substrate in order to minimize environ- mental noise.

Training Dataset

Data Collection We printed 33 weld beads of lengths 100 mm using the Inconel 718 (BOHLER 3D print AM 718) wires using a different combination of torch speed and wire feed rate to obtain different weld bead geometry. The torch speed and wire feed rate used to span the entire material process map and were in the range of [1,20] mm/s and [2,8] m/min, respectively.

Table 1: Process parameters used for printing

Torch Speed	Wire Feed Rate	Torch Speed	Wire Feed Rate	Torch Speed	Wire Feed Rate
10	4.5	7	4.5	10	8.5
9	4.5	5	4.5	9	8.5
8	4.5	17	2.5	8	8.5
12	2.5	6	4.5	10	3.5
15	2.5	10	6.5	10	5.5
1	2.5	9	6.5	10	7.5
1	4.5	8	6.5	20	2.5
2	2.5	7	6.5	7	8.5
3	3.5	6	6.5	6	8.5
2	3.5	5	6.5	5	8.5
3	4.5	4	4.5	10	2.5

All different combination of process parameters to print 33 beads are shown in the Table 1. We used around 70% Ar and 30% He as our shielding gas with a constant gas flow rate of around 25 L/min. We set the nozzle to deposit the material at around 15 mm above the substrate surface. We collected point cloud data of the printed beads using the GOM ATOS III Triple scanner. Next, we separated all the beads from the substrate using RANSAC plane segmentation. Then, we divided each bead into N = 20 segments, with each segment measuring about 5 mm. Similarly, we collected acoustic signals at 44 kHz during the printing process and segmented each bead signals into 20 acoustic signal segments, with each segment containing the acoustic signal for a 5 mm bead segment. Thus, with 33 beads, we get a total of 660 signal data segments.

Table 2: Time-domain features

Features	Formula	Features	Formula
Root Mean Square Pressure (RMSP)	$P = \sqrt{1/T \int_{i=0}^{T} p^2(t)dt}$	ZCR	$ZCR = \frac{f}{N}\sum_{i=1}^{N} \lvert sgn(x(n)) - sgn(x(n-1)) \rvert$
Energy	$E = \frac{1}{N}\sum_{i=1}^{N} {x_i}^2$	Crest Factor	$CF = \frac{\max \lvert x_i \rvert}{\sqrt{\frac{1}{N}\sum_{i=1}^{N} {x_i}^2}}$
Mean Amplitude	$A = \frac{1}{N}\sum_{i=1}^{N} \lvert x_i \rvert$	Peak-to-Peak	$y = \max(x) - \min(x)$
Kurtosis	$Kr = \frac{\frac{1}{N}\sum_{i=1}^{N}(x_i - \overline{x})^4}{\sigma^4}$	Impulsion Index	$I = \frac{x_m}{\overline{x}}$
Skewness	$SK = \frac{1}{N}\sum_{i=1}^{N}\left(\frac{x_i - x}{\sigma}\right)^3$	Mean	$M = \frac{1}{N}\sum_{i=1}^{N} x_i$
Standard Deviation	$STD = \sqrt{\frac{1}{N-1}\sum_{i=1}^{N}(x_i - \overline{x})^2}$	Shape Factor	$S_f = \frac{x_{rms}}{\overline{x}}$

Labeling: For dataset labeling, we follow the procedure of our published paper [10]. According to the paper, we consider three parameter metrics namely range curvature RC, maximum height MH, and range power RP. First, we collect point cloud scan data and acoustic signals for all bead segments. Next, for each bead segment, we extract the parameter metrics used for labeling. From the point cloud, i) we compute the mean curvature at each point in that segment, followed by the range of all these mean curvatures, RC; and ii) we compute the bead segment maximum height, MH. Similarly, from the acoustic signal, we compute the instantaneous power of its sound intensity, followed by the range of its instantaneous power, RP. Then, we perform a heuristic search to determine the optimal thresholds to separate the bead segments based on the proposed parameter metrics. This is a two-step procedure where we search through various threshold values that separate the bead segments and determine a candidate threshold that minimizes the overlapping area between their associated Kernel Density Estimation (KDE). Finally, we combine the various optimal parameter metrics thresholds to label geometrically good and defective segments. We consider all bead segments are bad above these thresholds. Otherwise, they are good. For more details refer to [10].

After labeling the dataset, we extract the previously mentioned (Table 2) time domain features from the training acoustic signals. To test the performance of the models, we use 10 fold stratified cross-validation approach, and the results of the models will be discussed in the next Section. Then we use all the training datasets for training the models and save the trained models for later use.

Testing Dataset

We printed two raster printing to verify the performance of our trained models on new datasets.

Single-layer Multi-Bead: Figure 3 shows our testing multi-bead printing where 6 consecutive beads are printed together using the Inconel 718 (BOHLER3D print AM 718). The length of each bead is around 100 mm. We use a constant TS=5 mm/s and WFR=6.5 m/min for printing all the beads except for the yellow rectangle region in the 4th bead, where we set the WFR=4.5 m/min. Since we change the WFR in this region, it creates a non-uniform printing that we consider defective printing. Other parameters, such as gas flow rate, and distance of the nozzle to the deposition plate are the same as the training dataset.

We collected acoustic signals at 44 kHz during the printing process and segmented the entire audio data into 120 segments so that each bead can be divided into 20 segments. Then we extracted time domain features from the signals and passed those features into our trained models.

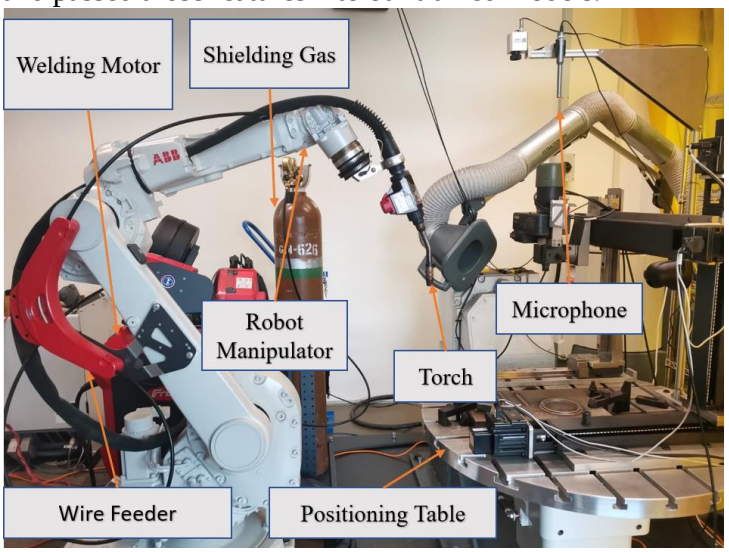

Figure 2: Experimental setup of SUTD Robotic WAAM for Bead Printing and Acoustic Data Collection

Multi-layer Multi-Bead: We printed 6 layers' multi-bead block whose length, thickness, and height are around 80 mm, 20 mm, and 15 mm respectively. Figure 4 shows the top layer of a multi-bead multi-layer printing of Inconel material. We used a constant TS=12 mm/s and WFR=6.5m/min for printing all the beads. We divided the audio of each bead into 10 segments. Therefore, for each layer, we get 100 audio segments and for total 6 layers, we get 600 audio signals.

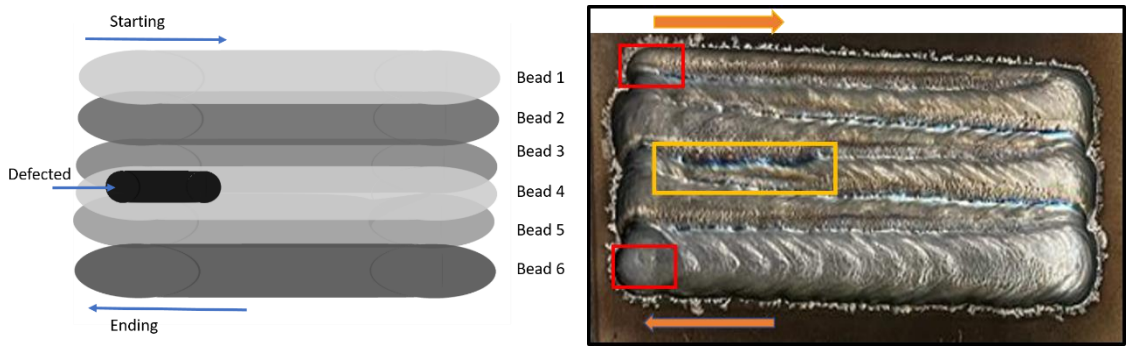

Figure 3: Schematic representation of single-layer multi-bead printing (left) and Actual printing (right). We intentionally induce a new WFR at the 4th bead lower part indicating a yellow rectangle.

Figure 4: Schematic representation of top layer of a multi-layer multi-beads printing (left) and Actual printing (right).

From Figure 4, the yellow rectangle indicates a void that occurs at the joining of two bead segments (starting segment of one bead and ending segments of another bead). The void is created unintentionally. Again some segments of beads also non-uniform.

Results and Discussion

Performance Evaluation of Defect Detection Models

In this section, we report and discuss about the performance of our trained models on single beads, single layer multi-bead and multi-layer multi-bead prints.

Single beads: Table 3 shows the comparative accuracy of the various models based on single beads. From the table, it can be seen that the combinatorics of time domain features and three ML models can be able to identify geometrically defective segments accurately with accuracy that ranges from 85% to 87%.

Table 3: Comparative study of defect identification models based on accuracy

Models	Accuracy
Time+KNN	85±0.02
Time+SVM	85.24±0.03
Time+RF	86.96±0.03

Single-layer Multi-Bead: Figure 5 shows the prediction results of the single-layer multi-bead printing using our previously trained models. From the figures, we observe that all the models can pick out the

defective region and predict the last segment as defective which we did not intentionally induce. In addition, the Time+SVM model can pick out all defected areas and the starting and ending segments. Though some good segments are falsely identified as bad by the trained models, the percentage is low that is around less than 7%. Overall, the prediction accuracy for single-layer multi-bead printing is above 90%. Therefore, we can conclude the trained models can pick out both the defective and defect-free segments.

Multi-layer Multi-Bead: Figures 6, 7 and 8 show the predicted results of multi-bead multi-layer printing using Time+KNN, Time+SVM and Time+RF models, respectively. The figures show that all the models can pick out the voids created in layers 5 and 6. In addition, all the models can pick out some obvious bad segments created randomly during printing. From the original images of different layers, we observe that layer 1, 2 and 3 looks more uniform than layers 4, 5 and 6. And our trained models also pick out more bad segments in layers 4, 5 and 6. Overall, the Time+SVM model can pick out more bad and good segments accurately than others. However, all models falsely pick out some good segments as bad that percentage is less than 10%. Therefore, we can conclude the trained models can pick out both the defective and defect-free segments.

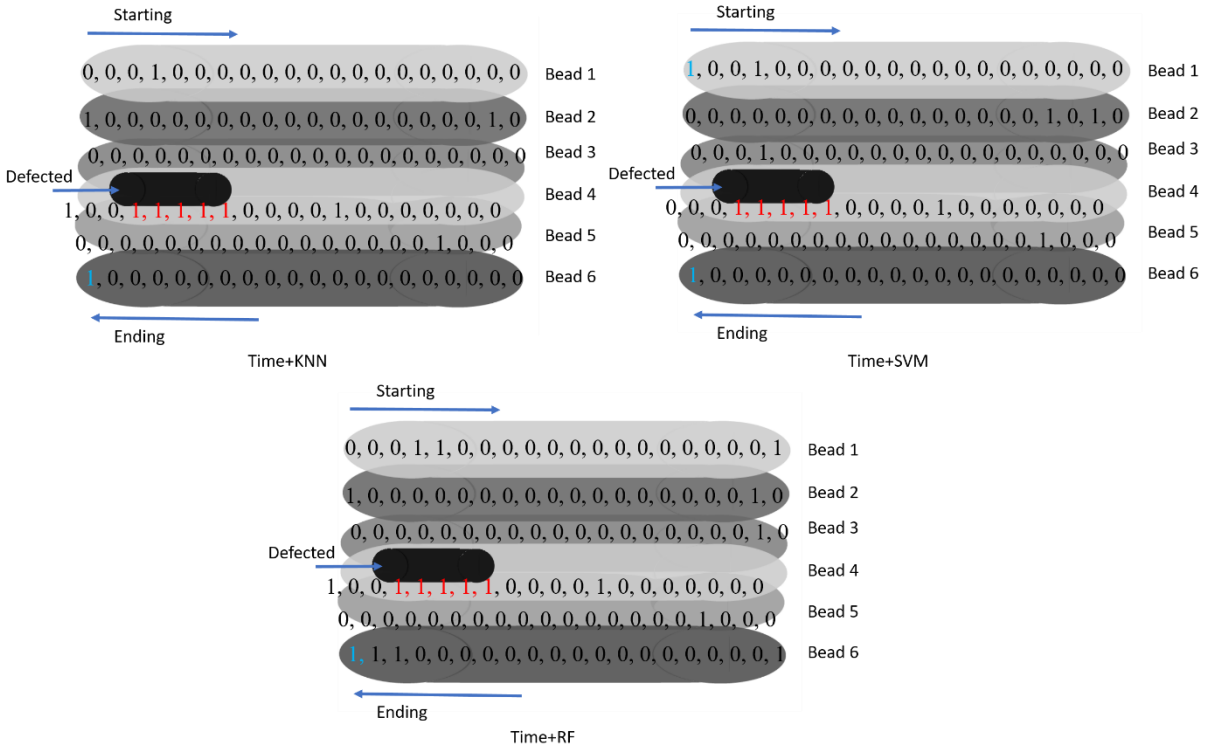

Figure 5: Prediction of single-layer multi-bead defect detection on its schematic representation. 1 indicates bad and 0 indicates good. Red 1 represent obvious defect and blue 1 represent the possibility of a defect.

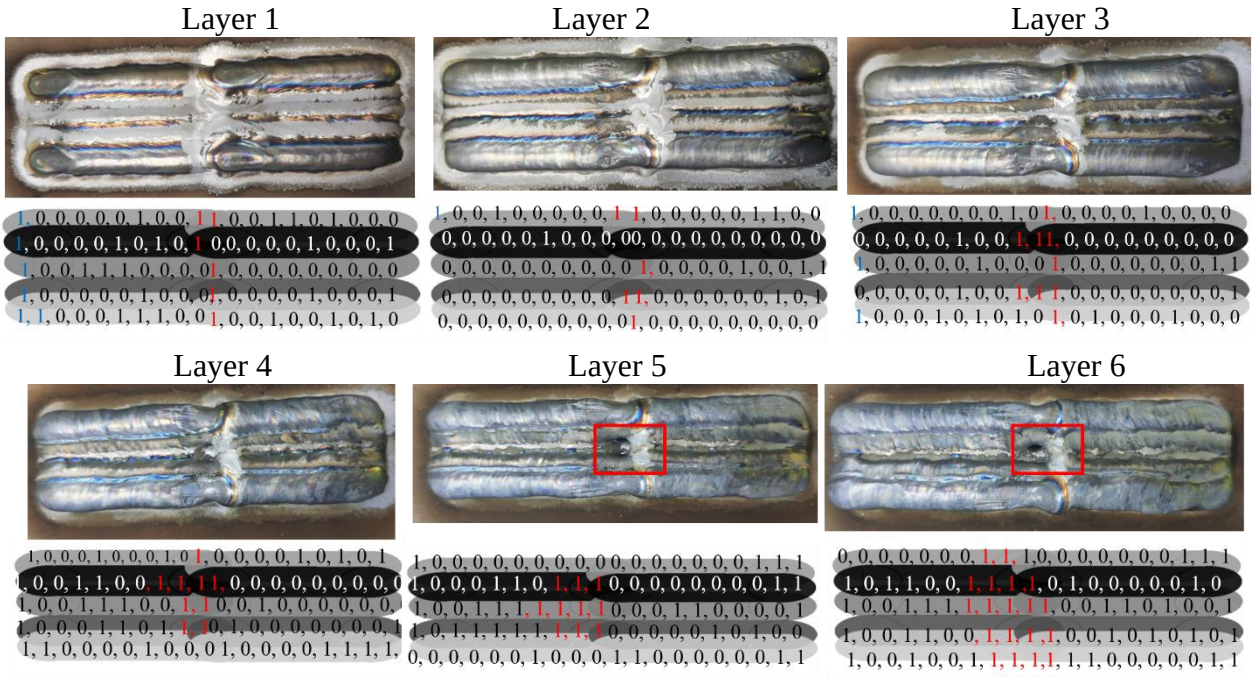

Figure 6: Prediction of multi-layer multi-bead defect detection using Time+KNN model on its schematic representation. 1 indicates bad and 0 indicates good. Red 1 represent obvious defect and blue 1 represent the possibility of a defect.

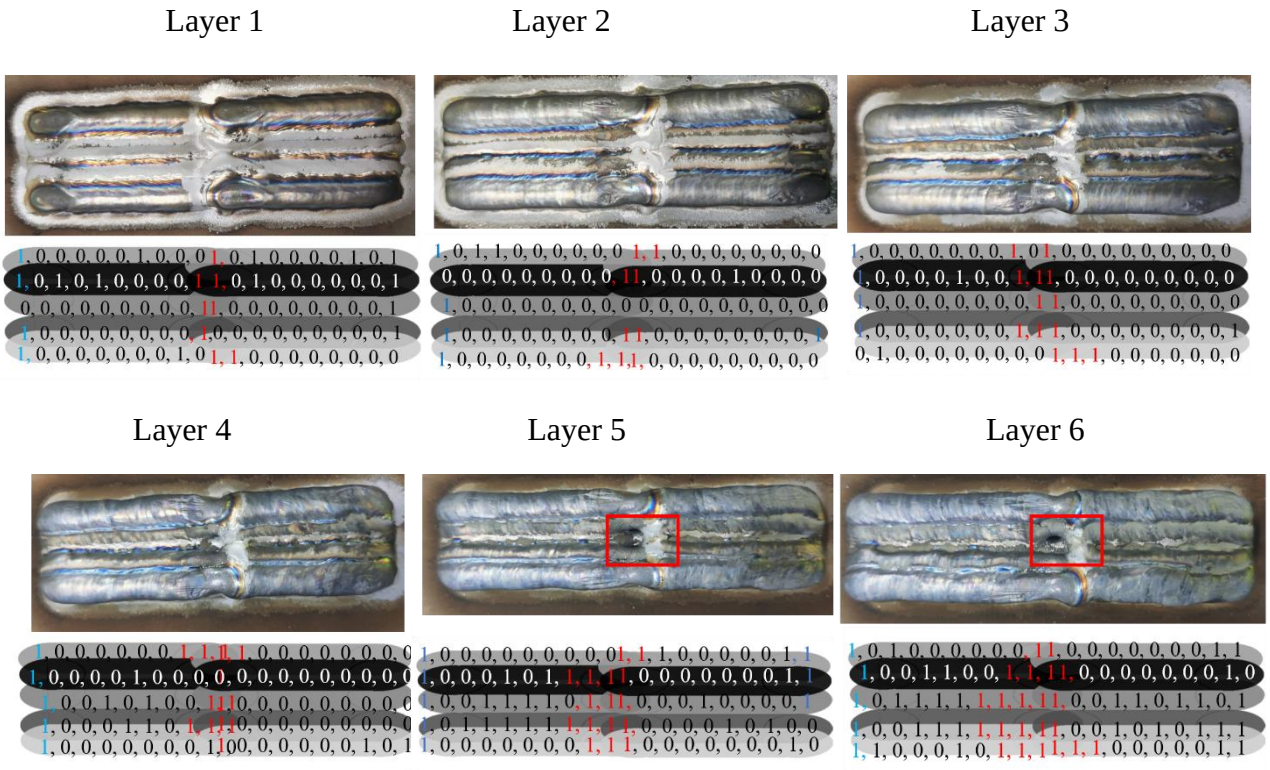

Figure 7: Prediction of multi-bead multi-layer defect detection using Time+SVM model on its schematic representation. 1 indicates bad and 0 indicates good. Red 1 represent obvious defect and

blue 1 represent the possibility of a defect.

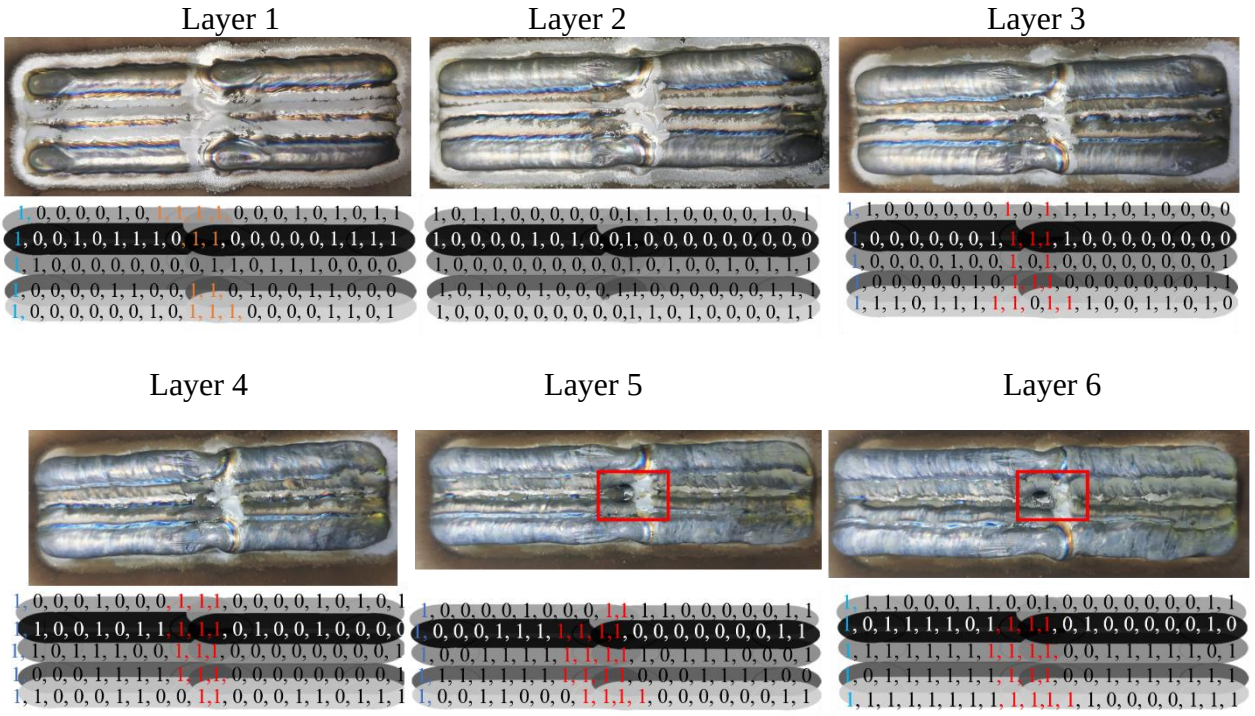

Figure 8: Prediction of multi-bead multi-layer defect detection using Time+RF model on its schematic representation. 1 indicates bad and 0 indicates good. Red 1 represent obvious defect and blue 1 represent the possibility of a defect.

Conclusion

In this paper, we investigate the performance of our previously proposed single-bead segments-trained defect detection machine learning (ML) models' scalability for identifying voids in the multi-bead prints for the WAAM process. We explore three-time domain feature-based trained models based on Inconel 718 datasets. The models are trained using various time domain features from the acoustic signals and the labels of the features are determined based on a heuristic search thresholds approach. The accuracy of the single bead-based models ranges from 85% to 86%. To verify the performance of the trained models on new datasets, we print one single-layer multi-bead and one multilayer multi-bead printing for testing. The results of the multi-bead printing show that the single bead segments-based defect identification models can identify defective and non-defective segments for single-layer multi-bead printing and multilayer multi-bead printing effectively. Our objective is to identify defects, and our models have proven adept at detecting all problematic segments. However, a significant limitation of our current defect detection approach lies in its occasional misclassification of good segments as bad. In our future research, we intend to mitigate this issue by incorporating data from a range of multimodal sensors, such as vision and thermal sensors, into the training process for individual bead segments. We hypothesize that leveraging multiple sensor inputs will substantially

enhance the precision of our single-bead inspections, thereby reducing the occurrence of false positives when deploying our trained models for multi-bead testing.

Acknowledgment

The authors gratefully acknowledge the support of the Growth Plan Grant for Aviation at the Singapore University of Technology and Design.

References

[1] Alessandro Busachi et al. "Designing a WAAM based manufacturing system for defence applications". In: *Procedia Cirp* 37 (2015), pp. 48–53.

[2] Donghong Ding et al. "A practical path planning methodology for wire and arc additive manufacturing of thin-walled structures". In: *Robotics and Computer-Integrated Manufacturing* 34 (2015), pp. 8–19.

[3] Almir Heralic. *Monitoring and control of robotized laser metal-wire deposition*. Chalmers University of Technology, 2012.

[4] Paul Kah and J Martikainen. "Influence of shielding gases in the welding of metals". In: *The International Journal of Advanced Manufacturing Technology* 64 (2013), pp. 1411–1421.

[5] Na Lv et al. "Real-time control of welding penetration during robotic GTAW dynamical process by audio sensing of arc length". In: *The International Journal of Advanced Manufacturing Technology* 74.1-4 (2014), pp. 235–249.

[6] Kamal Pal, Sandip Bhattacharya, and Surjya K Pal. "Investigation on arc sound and metal transfer modes for on-line monitoring in pulsed gas metal arc welding". In: *Journal of Materials Processing Technology* 210.10 (2010), pp. 1397–1410.

[7] Ivan Polajnar, Zoran Bergant, and Janez Grum. "Arc Welding Process Monitoring by Audible Sound". In: *12th International Conference of the Slovenian Society for Non-Destructive Testing: Application of Contemporary Non-Destructive Testing in Engineering, ICNDT 2013-Conference Proceedings*. 2013, pp. 613–20.

[8] Nowrin Akter Surovi, Audelia G Dharmawan, and Gim Song Soh. "A Study on the Acoustic Signal Based Frameworks for the Real-Time Identification of Geometrically Defective Wire Arc Bead". In: *International Design Engineering Technical Conferences and Computers and Information in Engineering Conference*. Vol. 85383. American Society of Mechanical Engineers. 2021, V03AT03A003.

[9] Nowrin Akter Surovi, Shaista Hussain, and Gim Song Soh. "A Study of Machine Learning Framework for Enabling Early Defect Detection in Wire Arc Additive Manufacturing Processes". In: *International Design Engineering Technical Conferences and Computers and Information in Engineering Conference*. Vol. 86229. American Society of Mechanical Engineers. 2022, V03AT03A002.

[10] Nowrin Akter Surovi and Gim Song Soh. "A heuristic approach to classify geometrically defective bead segments based on range of curvature, range of sound power and maximum height". In: *International Design Engineering Technical Conferences and Computers and Information in Engineering Conference*. American Society of Mechanical Engineers. 2023.

[11] Nowrin Akter Surovi and Gim Song Soh. "Acoustic feature based geometric defect identification in wire arc additive manufacturing". In: *Virtual and Physical Prototyping* 18.1 (2023), e2210553.

[12] Nowrin Akter Surovi and Gim Song Soh. "Process map generation of geometrically uniform beads using support vector machine". In: *Materials Today: Proceedings* 70 (2022), pp. 113– 118.

[13] Yaowen Wang and Pensheng Zhao. "Noncontact acoustic analysis monitoring of plasma arc welding". In: *International journal of pressure vessels and piping* 78.1 (2001), pp. 43–47.

[14] Bintao Wu et al. "A review of the wire arc additive manufacturing of metals: properties, defects and quality improvement". In: *Journal of Manufacturing Processes* 35 (2018), pp. 127–139.

[15] Chunyang Xia et al. "A review on wire arc additive manufacturing: Monitoring, control and a framework of automated system". In: *Journal of Manufacturing Systems* 57 (2020), pp. 31– 45.

[16] Fangda Xu et al. "Realisation of a multi-sensor framework for process monitoring of the wire arc additive manufacturing in producing Ti-6Al-4V parts". In: *International Journal of Computer Integrated Manufacturing* 31.8 (2018), pp. 785–798.